Impacts of Sea-Level Rise on Hypoxia and Phytoplankton Production in Chesapeake Bay: Model Prediction and Assessment

Xun Cai (iD)*, Jian Shen* (iD)*, Yinglong J. Zhang* (iD)*, Qubin Qin* (iD)*, Zhengui Wang, and Harry Wang*

Research Impact Statement: This modeling study on the impacts of sea-level rise on the seasonal hypoxia and phytoplankton production in Chesapeake Bay helps us better understand the mechanisms that drive the changes.

ABSTRACT: In this study, the influence of sea-level rise (SLR) on seasonal hypoxia and phytoplankton production in Chesapeake Bay is investigated using a 3D unstructured grid model. Three SLR scenarios (0.17, 0.5, and 1.0 m) were conducted from 1991 to 1995. Results show that the summer hypoxic volume (HV) increases about 2%, 8%, and 16%, respectively, for these three scenarios, compared with Base Scenario. The contributions of physical and biological processes on the increase in the HV were analyzed. With the projected SLR, enhanced gravitational circulation transports more oxygen-rich water in the bottom layer from the mouth. However, the pycnocline moves upwards along with increasing water depth, which largely prolongs the time for dissolved oxygen (DO) to be transported to the bottom. The altered physical processes contribute greatly to a larger HV baywide. Besides, SLR increases the whole Bay phytoplankton production, with a larger increase in shallow areas (e.g., 53% in areas with depth <1 m under SLR of 0.5 m). Enhanced light availability is suggested to be the major driver of blooming phytoplankton under SLR in shallow areas. While increased DO production over the euphotic zone is mostly released to the atmosphere and transported downstream, the increase in settled organic matter greatly promotes DO consumption in the water column. The increased respiration is another major cause of the HV increase besides the physical contributions.

(KEYWORDS: sea-level rise; hypoxia; phytoplankton production; Chesapeake Bay; modeling; SCHISM.)

INTRODUCTION

Hypoxia (dissolved oxygen [DO] concentration ≤2 mg/L), occurs in deeper regions of Chesapeake Bay (the Bay hereafter) in the summertime and has been recorded since the last century (Seliger et al. 1985; Hagy et al. 2004). The hypoxic volume (HV) in Chesapeake Bay ranges from 8 to 17 km^3, with larger HV observed in wet years (Hagy et al. 2004; Bever et al. 2013). The observed large HV decreases habitats for fish, invertebrates, and benthic macrofauna and therefore degrades the ecosystem by changing the food web and energy transfer between different trophic levels (Diaz and Rosenberg 1995; Vaquer-Sunyer and Duarte 2008). Besides, hypoxia changes nutrient cycling by inducing bottom nutrient release that further affects the ecosystem (Kemp et al. 1990).

The primary cause of hypoxia in the Bay is that DO consumption exceeds replenishment from the surface waters through the pycnocline. Net planktonic respiration, heterotrophic respiration, and benthic consumption of deposited organic matter are major components of the bottom water DO consumption

(Kemp et al. 1992). The DO replenishment from the atmosphere decreases when the vertical stratification is strengthened and the solubility is reduced in warmer water in summer (Taft et al. 1980). For example, an increase in freshwater discharge from the Susquehanna River, which also brings excess nutrients, leads to a stronger stratification and therefore severe hypoxia (Taft et al. 1980; Seliger et al. 1985). Excessive anthropogenic loads of nutrients are recognized to be a major cause of eutrophication. The onset of hypoxia in the Bay usually starts after the spring algal bloom and the subsequent respiration of settled and enhanced accumulation of organic matter in the water column and bottom sediment (Newcombe and Horne 1938; Murphy et al. 2011). After the initiation of hypoxia, increased nutrient flux from the sediment supports the summer algal bloom which further increases the bottom water column DO consumption (Kemp et al. 1992; Murphy et al. 2011).

Worldwide sea-level rise (SLR) has been accelerating over recent years from about 1.7 mm/year between 1901 and 2010 to about 3.2 mm/year between 1993 and 2010 (IPCC 2007). In Chesapeake Bay, the estimated trend of relative SLR, varying from 2.7 to 4.6 mm/year for different locations over 1955 to 2007, is larger than the estimation for global mean SLR (Zervas 2001; Boon et al. 2010). SLR is projected to be 0.3–0.7 m by 2050 and 0.7–1.6 m by 2100 (Rahmstorf 2007; Najjar et al. 2010; Boesch et al. 2013). Under SLR, the bay-averaged salinity is predicted to increase by 0.5 with an SLR of 0.2 m (Hilton et al. 2008). The bay-averaged stratification is estimated to be strengthened under SLR, which reduces vertical exchange through the pycnocline and tends to diminish the bottom DO supply from the surface layer (Hong and Shen 2012). Additionally, the residence time for substances discharged from the Susquehanna River is prolonged due to larger water volume under SLR (Hong and Shen 2012). The changes in hydrodynamics could affect DO dynamics and HV.

Multiple numerical studies have been conducted to discuss the change in the hypoxic/anoxia volume in response to SLR in the Bay. However, diverse changes have been predicted. Both Wang et al. (2017) and Irby et al. (2018) showed an improvement in the DO conditions whereas Ni et al. (2017) suggested an increase in the summer HV. St-Laurent et al. (2019) made an explicit comparison between different models and showed that all the models predict the same trend of change in DO but disagree on the changes in HV. This suggests large uncertainties still exist in numerical modeling of the effects of SLR on hypoxia. The uncertainties may be largely due to the differences in model kinetic parameters and grid resolution. Another concern is the lack of a high-resolution

grid that cannot well represent shallow waters and tributaries in many of these models (Cai et al. 2020). There has been no report on what and how much change will happen in shallow regions under SLR, though tributaries and shallow water areas (water depths smaller than 2 m in this study) are expected to experience larger changes compared with the main stem of the Bay.

In this study, a high-resolution three-dimensional unstructured-grid (UG) model is used to investigate the effects of SLR on hypoxia. Besides studying the effects of SLR on the main stem, we also explore the changes in HV, flushing time, and phytoplankton production, with a focus on the tributaries and shallow water areas. This paper is organized as follows: a description of the model, scenarios, and analysis methods are presented in Methods. Results of changes in hypoxic conditions and phytoplankton production are presented in Results. Discussion presents the discussions on the drivers of the changes for hypoxia including inside the tributaries and shallow water areas. The last section summarizes the entire study.

METHODS

SCHISM-ICM

We use a fully coupled hydrodynamic and water quality model, Semi-implicit Cross-scale Hydroscience Integrated System Model with the Integrated Compartment Model (SCHISM-ICM), which couples the SCHISM-ICM for water quality simulation (Cerco and Cole 1994; Zhang et al. 2016; Cai et al. 2020; schism.wiki). In addition, the sediment flux model which simulates the diagenesis and recycling processes is incorporated into ICM (Di Toro and Fitzpatrick, 1993). SCHISM-ICM solves physical and biogeochemical processes simultaneously. There are 21 water quality state variables simulated by ICM: three algal assemblages, comprised of diatom, green algae, and cyanobacteria, along with three groups of carbon, five groups of nitrogen, four groups of phosphorus, chemical oxygen demand, and DO. Local kinetic processes of these state variables are simulated by ICM, whereas transport and spatial distribution of these state variables are simulated by SCHISM.

SCHISM uses a semi-implicit time-stepping scheme applied in a hybrid finite-element and finite-volume framework to solve Navier–Stokes equations and uses an Eulerian–Lagrangian method to treat the momentum advection. This numerical scheme

ensures the time step is not restricted by the Courant–Friedrichs–Lewy condition. For shallow water areas where high-resolution model grids are used, the time step can remain large in the hydrodynamic model. This largely improves numerical efficiency. In the vertical dimension, the model uses a highly flexible and efficient hybrid coordinate system LSC2 (localized Sigma Coordinates with Shaved Cell), which allows a varying number of vertical grids at each node (Zhang et al. 2015). The high-resolution model grids, coupled with the hybrid vertical coordinate system for shallow water areas allow for seamless spatial cross-scale simulations. This makes it feasible to study the effects of SLR on shallow and deep areas as a whole.

Design of Scenarios

The model domain for Chesapeake Bay and its tributaries is shown in Figure 1. Base Scenario uses the current mean sea level as a reference datum for model simulations, and the model has been developed and calibrated by Cai et al. (2020). The simulation period is from 1991 to 1995, which is currently used as a reference period for management scenario simulations by the Chesapeake Bay Program (CBP). Besides the Bay proper, the grid extends farther offshore to the shelf break to minimize the influence of open ocean conditions on the interior of the Bay. The grid resolution varies from 2.4 km on the continental shelf to <100 m in tributaries. A flexible vertical grid system LSC2 developed by Zhang et al. (2015) was applied in this study, which preserves the spatial

variation of bathymetry in high fidelity. The number of vertical layers varies from 11 to 52 (33 on average) for the whole system with resolution varying from 0.5 to 19 m. The model uses a single nonsplit time step of 150 s.

Interpolated elevations from two tidal gauges at Lewes, Delaware, and Beaufort, North Carolina were used to force elevations at the ocean boundary. We obtained the boundary temperature from Simple Ocean Data Assimilation (Carton and Giese 2008) from January 1, 1991 to October 6, 1992 (when hybrid coordinate ocean model [HYCOM] is not available) and HYCOM (Chassignet et al. 2007) from October 7, 1992 to December 31, 1995. World Ocean Atlas monthly climatological data provided the ocean boundary salinity. We used constant values for the nutrients and other water quality variables in the ocean boundary because the ocean boundary is far away from the Bay mouth and the model simulation in the Bay was tested to be generally insensitive to the nutrient conditions at the ocean boundary (Cai et al. 2020). Phase 6 Watershed Model of Chesapeake Bay Assessment Tool provided daily runoff and nutrient loads from the watershed for this study (Shenk and Linker 2013). The daily loadings are linearly interpolated into each time step in this model. The atmospheric forcing and heat fluxes were obtained from the North American Regional Reanalysis (Mesinger et al. 2006).

SLR of 0.17, 0.5, and 1.0 m were added to the sea surface height at the ocean boundary of the Base Scenario, respectively, for each SLR scenario. All scenarios share identical oceanic, watershed, and atmospheric forcings. In this study, since we focus on
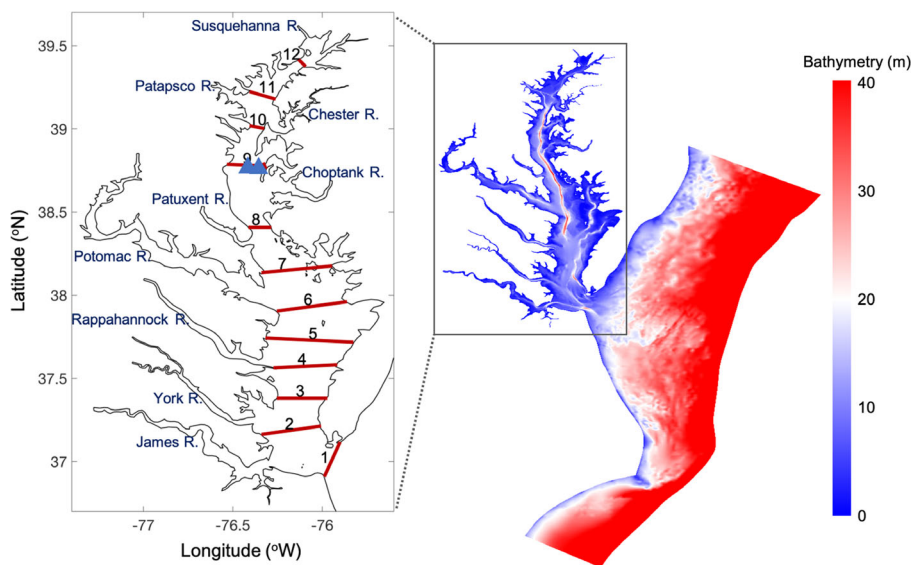

FIGURE 1. Model domain for Chesapeake Bay and its tributaries, with the 12 cross channel sections (red lines). Two blue triangles denote the locations used for vertical profile analysis.

the effects of SLR as the sole driver to cause changes in transport and biochemical processes, all other processes, such as river discharge, wind, solar radiation, and nutrient loadings remain unchanged.

According to estimations from Dettmann (2001), the surface area of the Bay is $11,524 \times 10^6$ m^2 and the mean depth of it is 6.8 m. SLR of 0.5 m will increase the Bay volume (ΔVol) by 5.764 km^3 (7.4%) without considering the changes in the surface area. The average volume or depth increase is 7.4% of the original total volume and depth. For this study, the increase in the surface area in the low-lying area of the Bay due to SLR was not considered for comparing the model results with other published model results.

Analysis Methods

Flushing Time. Flushing time is the time it takes to replace the water mass of a waterbody and is often estimated by the ratio of the mass of a scalar in a reservoir to the rate of renewal of the scalar (Monsen et al. 2002). We calculated the flushing time for the major tributaries because the river discharge is estimated to be dominant for the water exchange in the Chesapeake Bay (Xiong et al. 2021). Flushing time can be estimated numerically by calculating the e-folding time. To calculate the e-folding time, passive tracers were released in each tributary twice a month for a year. The e-folding time for each release was calculated as the time it takes for tracer concentration decreases to e^{-1} (about 37%) of the initial tracer concentration, and the values were then averaged for the year 1992 (Monsen et al. 2002).

Hypoxic Volume. The HV estimation follows the method in Bever et al. (2013) for estimating the HV based on observations. Using the same method helps avoid any bias introduced by the estimation method when comparing the modeled HV with observations. The modeled DO profiles at major CBP stations (as used by Bever et al. 2013) were interpolated/extrapolated onto the current SCHISM UG grid to cover the entire Chesapeake Bay before the total HV was calculated. A linear interpolation was used at each vertical layer, and the hypoxic layer thickness at each node was then calculated. The hypoxic layer thickness at each element is the averaged value among its three-/four surrounding nodes. The total HV is the sum of HV in each element, which is the product of the element area and its hypoxic layer thickness.

Phytoplankton Production. Local phytoplankton production was computed by integrating local phytoplankton production in each water column for the element:

$$\text{GPP} = \sum_{i=1}^{n} (\text{C1}_i \cdot \text{G1}_i + \text{C2}_i \cdot \text{G2}_i + \text{C3}_i \cdot \text{G3}_i) \cdot \text{dep}_i,$$

(1)

where GPP is areal gross primary production of phytoplankton (g C/m^2/day), n is the number of layers in each element, i is the vertical layer index, C1, C2, and C3 are carbon-based phytoplankton biomass of three groups (diatoms, green algae, and cyanobacteria) over each layer, respectively (g C/m^3), and G1, G2, and G3 are growth rates of the three phytoplankton groups (day^{-1}), and dep is layer thickness (m).

Comparison of DO Concentration and Local Change Rates. DO concentration and its local change rate were calculated based on the absolute altitude in each vertical layer of the model for both Base and SLR Scenarios. To better compare the vertical profiles of these values between Base and SLR Scenarios, two references in the vertical coordinate were used. The first reference was set to be the bottom, and its vertical position is unchanged in the model. This reference helps to estimate the changes in DO in the bottom hypoxic layer. The second reference was set to be the free water surface, which rises in each SLR Scenario. This reference helps to compare the contributions of local biological processes in the upper layer, such as phytoplankton growth.

Oxygen and Nutrient Fluxes. Oxygen and nutrient fluxes were calculated at 12 cross sections from the Bay mouth to the head (Figure 1). Influx and outflux were calculated as the sectionally integrated products of along-channel flow velocity and concentration of DO or nutrient where the velocity direction is upstream into the Bay (marked as negative) and downstream (positive), respectively. The calculations of fluxes through each cross section follows:

$$\begin{cases} \text{influx} = \int\limits_{A(u<0)} (u \cdot \text{Var})\text{d}A \\ \text{outflux} = \int\limits_{A(u>0)} (u \cdot \text{Var})\text{d}A \end{cases},$$

(2)

where u is the along-channel velocity (m/s), Var is DO or nutrient concentrations (g/m^3), A is the area of cross sections (m^2). Five-year averages of monthly and annually influx, outflux, and net flux at each cross section were then calculated.

RESULTS

DO under SLR

Changes in DO concentrations due to SLR (ΔDO; Δ = SLR Scenario − Base Scenario, thereafter) can be either positive or negative, where positive values of ΔDO mean increases in DO concentration after SLR and negative values mean decreases. For different SLR scenarios, ΔDO has different magnitudes but shows a similar distribution in general. The magnitude of ΔDO tends to increase linearly with the magnitude of SLR. The bottom ΔDO varies spatially, and it is mostly negative in shallow areas but becomes positive in some hypoxic areas (DO concentration is lower than 2 g/m^3) (Figure 2). From June to August, the bottom ΔDO approaches zero in the upper and mid-Bay (between latitude 38.5 and 39°N). A positive ΔDO of 0.1–0.2 g/m^3 can be seen in the region near 38°N when SLR exceeds 0.17 m.

The HV under SLR

HV generally increases (ΔHV > 0) with some inter-annual variations (Figure 3). Take the case of SLR = 0.5 m as an example, ΔHV ranges from 0.5 to 1.0 km^3 for different years. The increase in HV is positively correlated to the magnitude of SLR. ΔHV is, on average, about 2%, 8%, and 16% of the current HV in Base Scenario, respectively, for the scenarios of SLR of 0.17, 0.5, and 1.0 m. In addition, although

each case of SLR leads to a change in total water volume (ΔVol), ΔHV maintains a relatively stable fraction (10%–15%) of ΔVol.

As mentioned in the introduction, there are diverse predictions for ΔHV (Ni et al. 2017; Wang et al. 2017; Irby et al. 2018). Our predicted ΔHV has the same trend as Ni et al. (2017). St-Laurent et al. (2019) conducted a comparison between all the model predictions including the SCHISM-ICM model and showed the predicted trends of ΔDO are the same for all the models — positive ΔDO for the mid-lower Bay channel but negative for the shallow regions. The magnitude of ΔDO for each SLR scenario is comparable (St-Laurent et al. 2019). Our model result has a similar magnitude of ΔDO as ChesROMS-ECB (Irby et al. 2018), and lies between the CH3D-ICM (Wang et al. 2017) and UMCES-ROMS-RCA (Ni et al. 2017).

Phytoplankton Production under SLR

Changes in gross phytoplankton production (ΔGPP) have a significant impact on hypoxia in the Bay (Murphy et al. 2011). ΔGPP corresponding to SLR in the water column is positive in most areas of the Bay (Figure 4d, 4e). For shallow areas, the magnitude of ΔGPP can reach as high as 0.4 g C/m^2/day for the case of a 0.5 m SLR, i.e., a 50% increase in the phytoplankton production (Figure 4b, 4e). For the scenarios of 0.17 and 1.0 m SLR, the increases in the local production are up to about 18% and 80%, respectively (not shown in the figure). Large values of ΔGPP (e.g., >0.15 g C/m^2/day) generally occur in
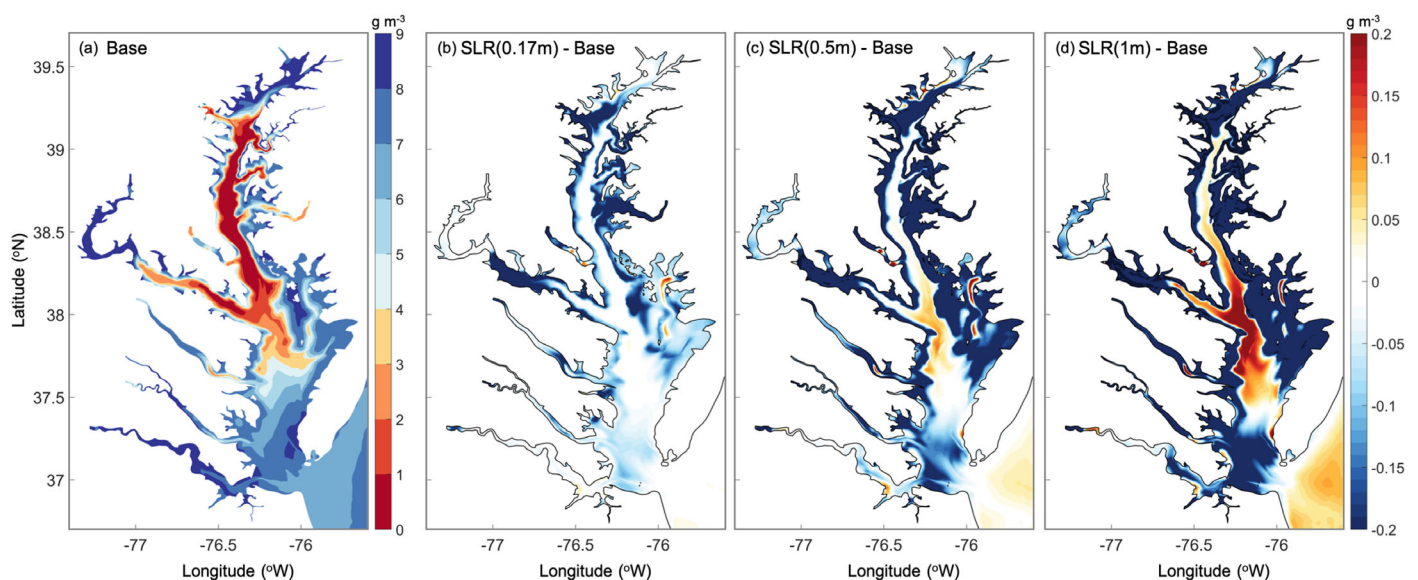

FIGURE 2. (a) Five-year averaged bottom dissolved oxygen (DO) concentrations in Base Scenario, and (b–d) absolute differences between sea-level rise (SLR) (0.17, 0.5, and 1 m) to Base Scenarios from June to August.
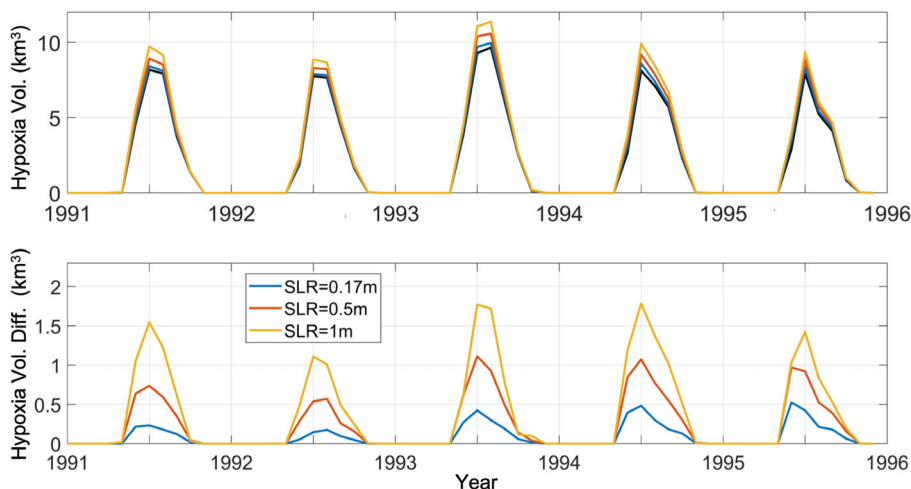
FIGURE 3. Hypoxic volume and difference under SLR scenarios of 0.17, 0.5, and 1.0 m. The black line in the upper panel is from Base Scenario.

shallow areas (<2 m) with relatively low values of GPP (e.g., <0.5 g C/m^2/day) in Base Scenario (Figure 4b, 4c). In tributary channels where the water depth ranges from 1 to 4 m, ΔGPP is up to 0.2 g C/m^2/day. In the deep areas (e.g., >8 m) where the GPP is large in Base Scenario (e.g., 0.8–1.4 g C/m^2/day), however, ΔGPP is much smaller and can even be negative (e.g., <0.02 g C/m^2/day) (Figure 4b, 4c).

High-depth-integrated chlorophyll-a concentrations (denoted by Tchla) are more concentrated in deep areas in the upper-middle part of the main Bay and deep tributaries such as the Potomac River (Figure 5a-1). In contrast, high depth-averaged chlorophyll-a concentrations (denoted by Mchla) are located in shallow areas in the upper-middle Bay regions, including shallow tributaries such as the Chester River (Figure 5d, 5g). Changes in depth-integrated chlorophyll-a concentrations (ΔTchla) generally show a similar spatial distribution as ΔGPP (Figure 5a-2, 5a-3). However, changes in depth-averaged chlorophyll-a concentrations (ΔMchla) can be both positive and negative over the Bay (Figure 5b-2, 5b-3).

DISCUSSION

The Contributions of Physical and Biochemical Processes to DO Dynamics under SLR

Physical Processes. SLR results in an increase in salinity throughout the Bay and the deep channel (Figure 6a). Bay-averaged ΔS is about 0.7 for the case of a 0.5 m SLR, and ΔS increases linearly with the magnitude of SLR. Results show that the length of salt intrusion also increases with SLR and the seasonal pattern agrees with predictions in Hong and Shen (2012). For example, a 0.5 m of SLR increases salt intrusion length by about 5 km on average (not shown). The increase in salinity and salinity intrusion suggests that more DO-rich coastal water can be transported into the Bay in the lower layer. This is supported by the upward oxygen at the 12 cross sections (Figure 7).

SLR drives stronger gravitational circulation, which inputs more oxygen-rich water into the lower layer of the Bay from the coast, and exports more oxygen in the upper layer (Figure 7). Although there is a net outflux of oxygen from the Bay annually (Figure 7a-3, 7b-3), the elevated bottom oxygen influx increases the bottom oxygen concentration over the lower Bay as shown in Figure 2b–2d. Compared with other model predictions for ΔDO in the Bay (e.g., Ni et al. 2017; Wang et al. 2017; Irby et al. 2018; St-Laurent et al. 2019), our model shows the positive ΔDO is more confined in the lower Bay due to the smaller influx of bottom oxygen at the location north to the Rappahannock Shoal (Cross section 5) (Figure 7b), which is different from other model predictions (St-Laurent et al. 2019). This smaller upstream transport shown in our model could result from the highly resolved bathymetry in SCHISM relative to other models (Cai et al. 2020).

The overall Bay-averaged stratification is strengthened with the enhanced gravitational circulation. Under SLR, the pycnocline rises *relative to the bottom* (Figure 6b). Meanwhile, the vertical salinity gradient (dS/dz) *relative to the sea surface* decreases, which indicates a slight increase in the mixing of DO near the surface (Figure 6c). However, this does not
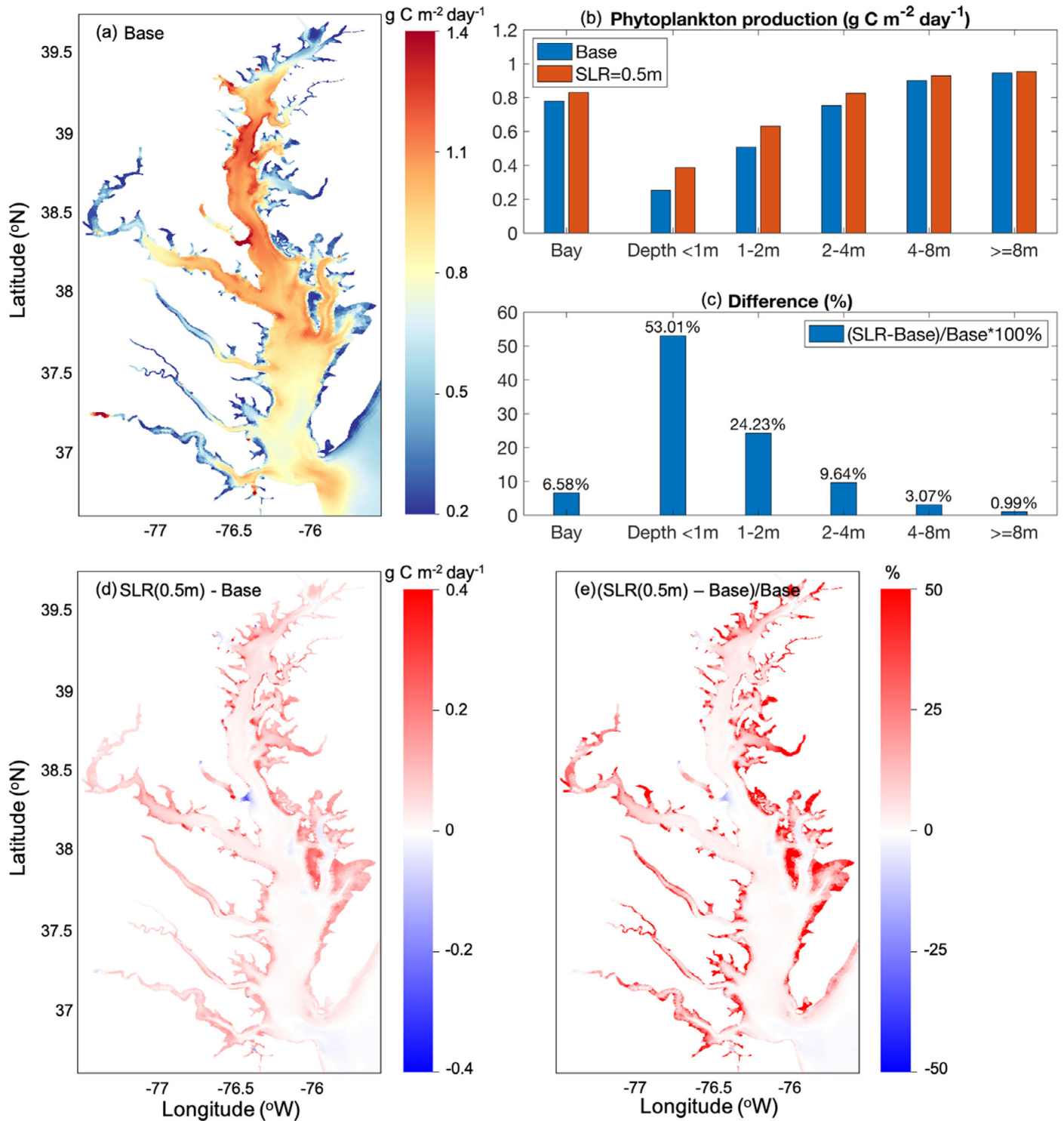
FIGURE 4. Five-year averages of gross phytoplankton production (depth-integrated) from April to June. (a) horizontal distribution in Base Scenario, (b) averages in areas of different water depths for Base Scenario and SLR = 0.5 m, (c) relative difference between Base Scenario and SLR = 0.5 m at different water depths, and horizontal distribution of (d) absolute difference and (e) relative difference caused by SLR = 0.5 m on Base Scenario.

necessarily mean that there is a higher DO flux transported from the upper layer into the lower layer of the water column. Previous studies suggest that

the time for water parcels transported from the surface to the bottom, the vertical exchange time, becomes longer in estuaries under SLR (Hong and

Depth-integrated Chlorophyll a Concentration (Tchla)

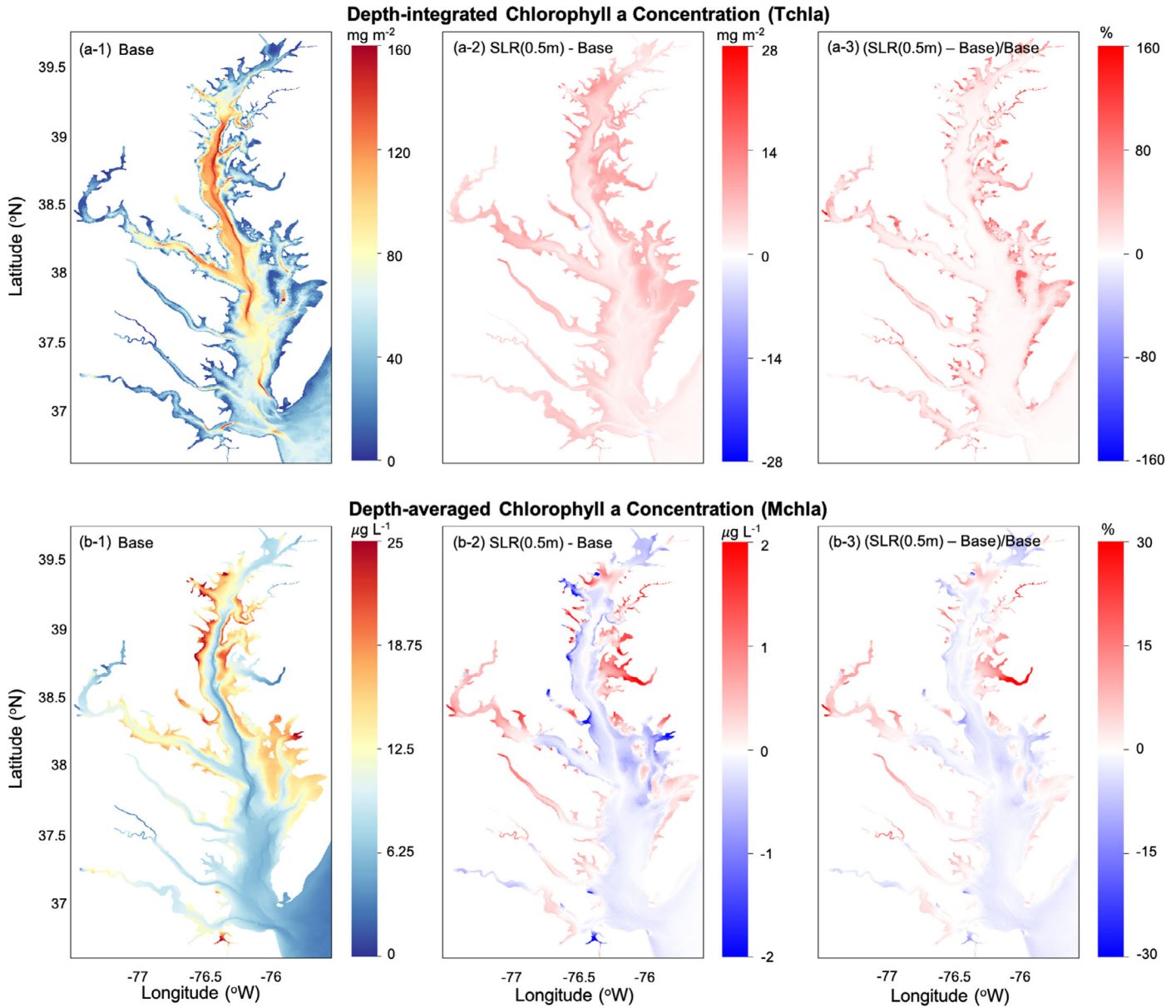## Depth-averaged Chlorophyll a Concentration (Mchla)

FIGURE 5. Five-year averages of (a) depth-integrated and (b) depth-averaged chlorophyll-a concentration from April to June, respectively, for (a,b-1) Base Scenario, (a,b-2) absolute difference and (a,b-3) relative difference caused by SLR = 0.5 m on Base Scenario.

Shen 2012). This is caused by the pycnocline rise and the increased volume below the pycnocline. Thus, although the mixing of DO may be enhanced above the pycnocline, the overall time required for the DO in the upper layer to be transported to the lower layer increases. As a result, the oxycline rises *relative to the bottom* under SLR (Figure 6d), which mainly drives the overall increase of HV (Figure 3). On the other hand, the DO concentration increases under SLR at the same distance below the surface (Figure 6e). This could be a result of enhanced mixing in the upper layer as discussed above, but could also be

a result of the increased phytoplankton production, which will be discussed in the next sections.

The contribution of lateral circulation is also studied. Under SLR, the increase in water depth in shallow areas is more pronounced than the deep channel, which can alter the lateral circulation. The model simulation shows that the lateral channel-shore exchange is strengthened along the lateral cross section under SLR. For example, the averaged surface velocity along the cross-channel direction over Section 9 (see Figure 1) increases 2.35% when SLR is 1 m. The increased channel-shore exchange is
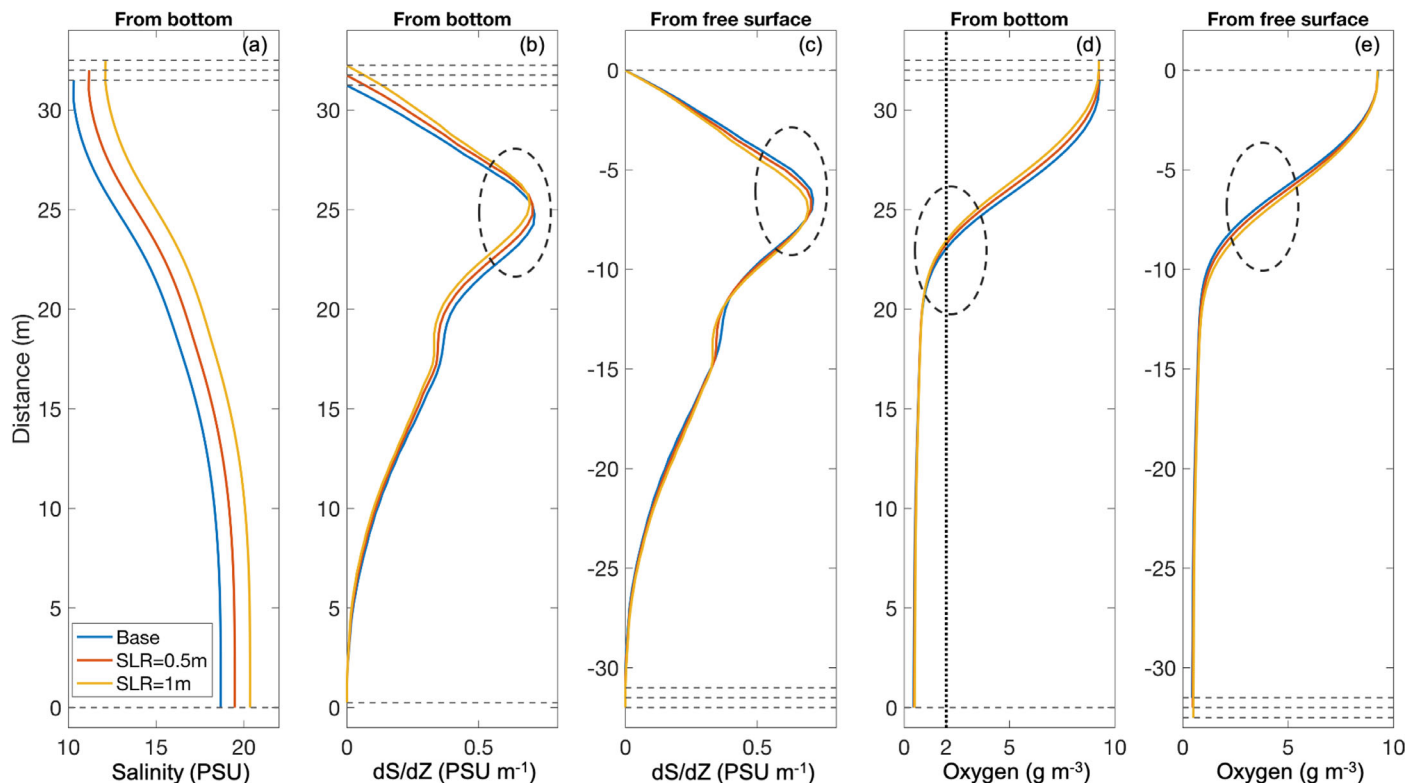
FIGURE 6. Five-year averages of the vertical distribution of (a) salinity (b,c) dS/dz, and (e,f) DO at a deep location in the hypoxic zone (Figure 1) from June to August. Profiles (a,b,d) relative to the bottom and (c,e) relative to the water surface are provided.

expected to transport more oxygen from shallow areas to deep channels to decrease HV. However, the lateral circulation-induced DO supply is minor, which is unable to offset baseline hypoxic conditions. On the other hand, the lateral advection of low-oxygen water contributes to the decrease in the bottom DO concentration in the shallow areas (Figure 2).

Biochemical Processes. The enhanced gravitational circulation, strengthened stratification, and increased water depth/volume caused by SLR, as discussed in Physical Processes Section, cannot fully explain the overall increased HV in the Bay since DO concentration increased in the deep channel of the mid-lower Bay. The model also suggests that the phytoplankton production increases under SLR, which produces more oxygen through photosynthesis, but consumes more DO through respiration. Surface DO for both deep (Figure 6d, 6e) and shallow areas (Figure 8a) changes little resulting from the air-sea equilibrium and advection. The local net rate of change in DO at the surface (1.1 g/m^3/day, Figure 8b) is smaller than the difference between DO production rate and respiration rate (1.7 g/m^3/day, Figure 8c, 8d), which suggests there is a net transport of DO from the water to the atmosphere. The outflux of DO by

gravitational circulation near the surface also increases. Therefore, more oxygen produced by the increased phytoplankton production under SLR does not help much to increase the bottom oxygen concentration. Furthermore, the settled organic matter, from increased phytoplankton production under SLR, contributes to more water column respiration (Figure 8d). The vertical distributions of local biochemical processes share the same trend as shown in Figure 8 for both deep and shallow areas. The increased phytoplankton production under SLR increases the settling of organic matter, resulting in the sediment oxygen demand. Also, the deepened water column and increased residence time prolong the retention time of increased organic matters in the water column, resulting in increased water column respirations.

DO Budget. We used a simple DO budget model to evaluate the contributions of both the physical transport and local biochemical processes to hypoxia in the region between Cross sections 7 and 8 (Figure 1), and quantitatively compared the contribution of each process for Base and SLR scenarios (Figure 9). The dominant processes are phytoplankton production, heterotrophic respiration, and net flux physical transport. Other processes, such as air-sea
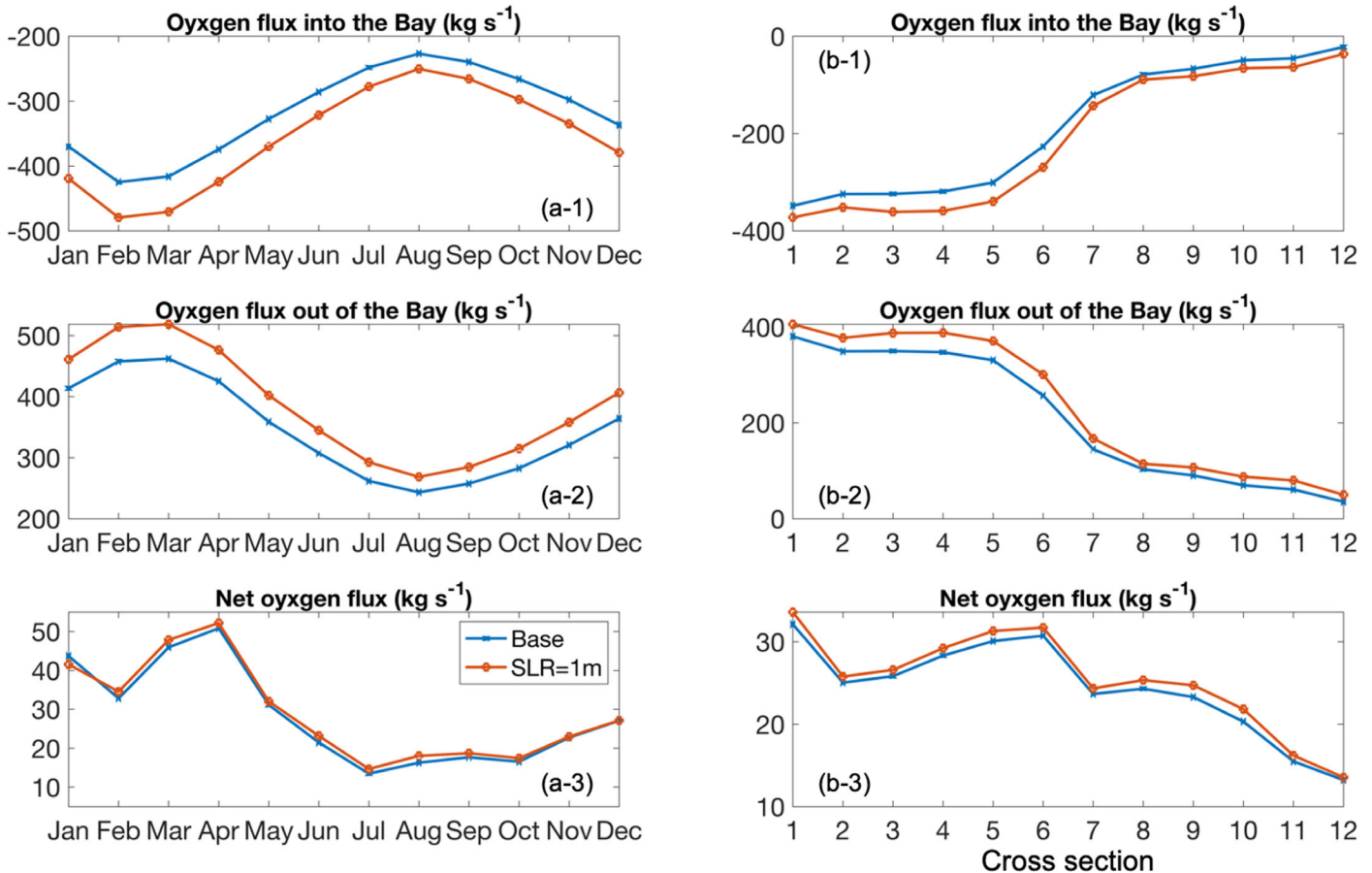
FIGURE 7. (a) Five-year averages of oxygen flux for each month from 1991 to 1995 at Cross section 4 near Rappahannock Shoal (Figure 1); (b) Five-year averages of annual oxygen flux from 1991 to 1995 at the 12 cross-sections from Bay mouth to head. Panels (a,b-1) are influx, panels (a,b-2) are outflux, and panels (a,b-3) are the net oxygen flux. Negative values mean flux into the Bay, whereas positive values refer to outflux.

exchange and nitrification, have relatively low contributions to the budget. Under SLR of 1 m, contributions of all dominant processes on DO budget increase. The total DO consumption increases by 11.2% (Figure 9b). Although the DO influx in the bottom layer increases under SLR (Figure 7), the increased net flux transports more DO out of the Bay. The increased total respiration and DO outflux overwhelm the increased DO production, which leads to more loss of DO and an enlarged HV.

Changes in Phytoplankton Production under SLR

Since both Tchla and local depth increase, the positive ΔMchla shown in certain areas indicates that the local production, especially the local growth, is enhanced due to the effect of SLR (Figure 5). In other areas, especially the main stem, the local Tchla is usually at a high level though ΔMchla is negative, implying that other local processes limiting the accumulation or growth of phytoplankton. For

example, Mchla is diluted by increased water depth. Also, the increased water depth and enhanced stratification reduce the upward flux of recycled nutrients from the lower layer, which reduces the nutrients supply in the surface layer for phytoplankton to take up.

The enhanced gravitational circulation affects both the transports of nutrients and phytoplankton. To quantify the export and retention of substances affected by SLR in the Bay, the freshwater age of the Bay was computed following the method in Shen and Haas (2004). The overall water age of the Bay increases with SLR. With an SLR of 0.5 m, the annual freshwater age of the Bay mouth increased by 20–60 days for different years from the value of about 200 days in Base Scenario (Cai et al. 2020). An increased freshwater age suggests that more nutrients will be retained inside the Bay for phytoplankton growth (Nixon et al. 1996), which is also supported by the changes in nutrient flux under SLR (Figure 10). The net outfluxes of both total nitrogen and dissolved inorganic nitrogen decrease in all the
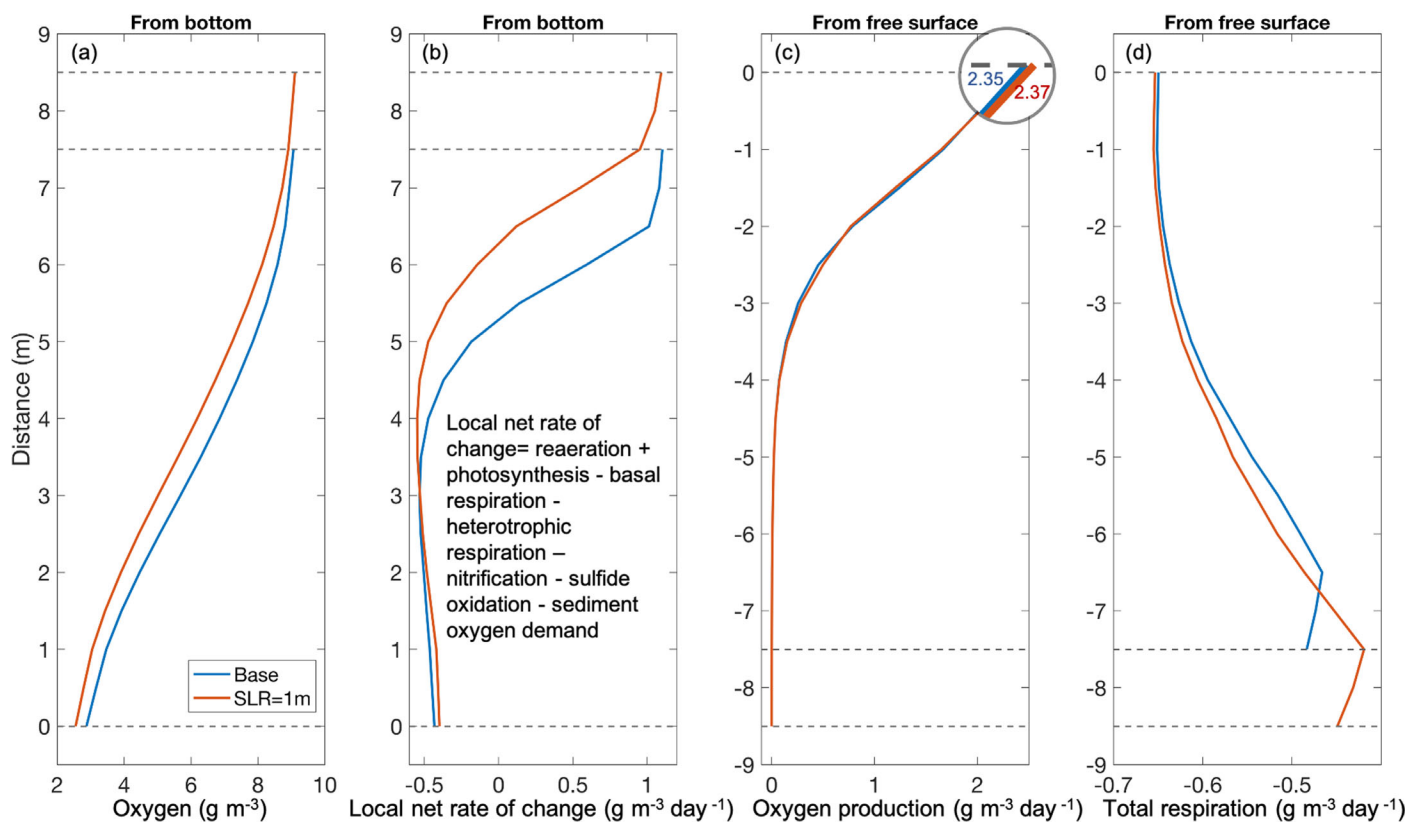
FIGURE 8. (a) Five-year averages of the vertical distribution of DO at a shallow location in Cross section 9 (Figure 1). (b) The local net rate of change resulting from the local processes controlling the DO budget, including reaeration, phytoplankton photosynthesis, basal respiration, heterotrophic respiration, nitrification, sulfide oxidation, and sediment oxygen demand. (c) The rate of local oxygen productions. (d) The rate of total local oxygen consumption, including basal respiration, heterotrophic respiration, nitrification, sulfide oxidation, and sediment oxygen demand. The averages are calculated for July.

seasons (Figure 10a-1,-2, 10b-1,-2); and the net influx of total inorganic phosphorus increases during most time of a year under SLR (Figure 10a-3, 10b-3). Besides, the Bay-wide stronger stratification tends to maintain phytoplankton in the euphotic zone.

Besides the direct effects on phytoplankton growth, accumulation and distribution, it appears that SLR reduces the growth limitations of phytoplankton in many tributaries or certain regions of large tributaries (e.g., the Choptank River, the upstream of the Potomac River). The changes in water volume (water column depth), transport and circulation, flushing time, as well as the nonlinear interactions among them, influence the local phytoplankton growth by changing the local nutrient and light availabilities, and the detailed discussion about these interactions will be presented in next Section.

Changes in Tributaries and Shallow Areas

Changes in Flushing Time of Major Tributaries. As discussed above, model results show that phytoplankton production increases significantly in tributaries and shallow areas under SLR. The increase in the GPP, however, is not proportional to the volume increase in most areas. Since nutrient loadings from the watershed are unchanged, the nutrient limitation for phytoplankton growth is mainly influenced by physical processes and nutrient consumption, and nutrient is less limited in tributaries. In this case, change in nutrient limitation under SLR for phytoplankton growth is expected to be minor in tributaries and shallow areas. Flushing time was computed for each major tributary to explore the local retention and dynamic processes that affect the dynamics of phytoplankton and nutrients.

Opposite to the situation that residence time of the Bay increases under SLR, the flushing time in most tributaries in the upper Bay (e.g., the Chester River) tends to decrease with SLR (Figure 11a); however, this seems a relatively minor factor (see discussions below).
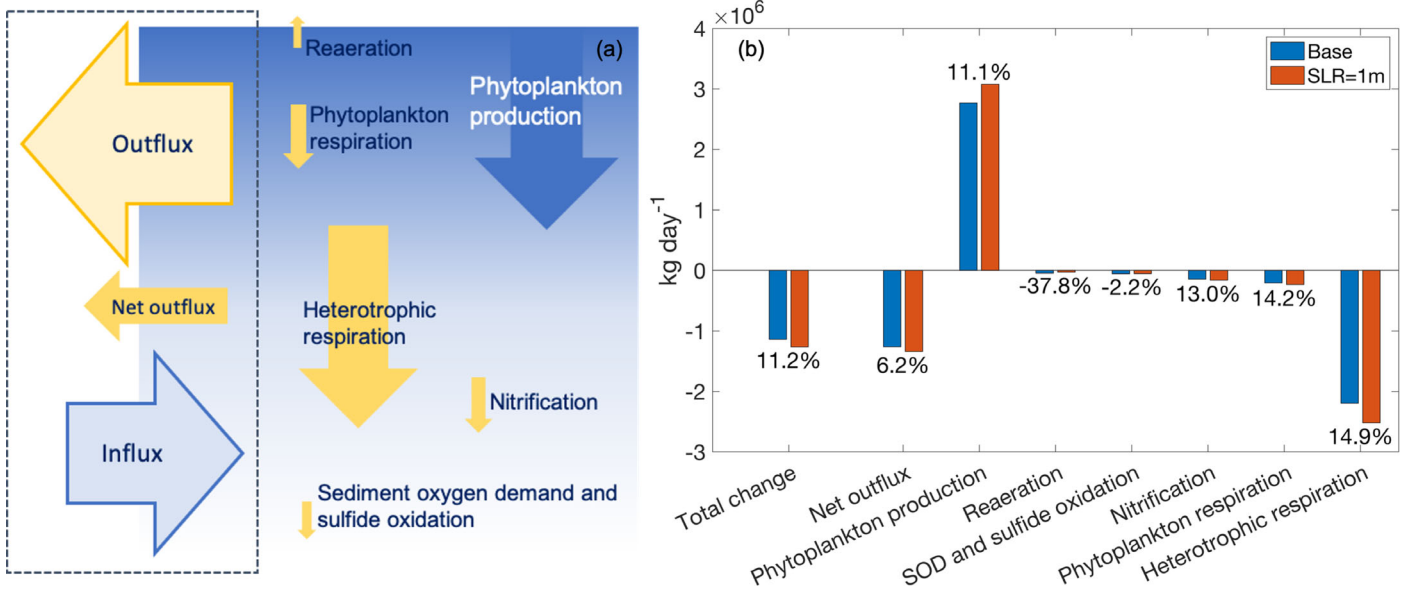
The flushing time of a tributary can be expressed as:

FIGURE 9. Five-year averages of the contribution of each physical or biological process to the DO budget in the area between Cross sections 7 and 8 (Figure 1) from June to August, for Base and SLR Scenarios. (a) Diagram of the contribution of each process to the DO budget, where the width of the arrow is generally proportional to the averaged contribution. Blue arrows indicate source terms of the DO budget and yellow arrows indicate sink terms of the DO budget. (b) Bar plots of each term in the DO budget, with the change percentages (SLR-Base)/Base labeled.

$$\tau = \frac{V}{Q}, \quad (3)$$

where V is the total volume and Q is the flux out of tributary (Monsen et al. 2002). The change in flushing time depends on the net effect of increases in volume and flux. Although SLR increases water volume, V, which tends to increase the flushing time, it also increases flux Q, as suggested by the classic estuarine circulation theory. According to the classic estuarine circulation theory (Hansen and Rattray 1966; MacCready and Geyer 2009), the velocity of the exchange flow is quantified by the expression:

$$u_E = \frac{g\beta \bar{s}_x H^3}{48 K_m}, \quad (4)$$

where g is the gravitational acceleration constant, $\beta \cong 7.7 \times 10^{-4}$ PSU^{-1}, $\bar{s}_x$ is depth-averaged salinity gradient in the along-channel direction, H is water depth, and K_m is the vertical eddy viscosity. The outflux can be expressed by the production of u_E and the cross-sectional area. This suggests that the increase of water depth increases both the velocity of the exchange flow and cross-sectional area. Therefore, the increase in water depth increases the water exchange and shortens the flushing time (Hansen and Rattray 1966; Shen and Lin 2006). Since the outflux can increase if the exchange flow increases due

to the enhanced gravitational circulation, the change in flushing time ($\Delta\tau$) depends on the competition between the increases in the volume and the increase in the flux resulting from increased gravitational circulation. $\Delta\tau$ can be either positive or negative for different tributaries.

Effects of Sea-Level Rise on Light Supply in Tributaries. The areal phytoplankton primary production is the integration of productivity over the water column. In estuaries, phytoplankton is distributed vertically in the upper mixed layer, whereas photosynthesis occurs in the euphotic zone. The ratio of the depth of the euphotic zone (1% of the surface irradiance) to the depth of the mixed layer can alter the light availability in the water column and hence regulate the areal phytoplankton production (Cloern 1987; Smith and Kemp 1995). In deep areas where the depth of the euphotic zone is greater than the depth of the mixed layer, light is fully utilized in the water column and leads to maximum phytoplankton production. However, in areas where the depth of the euphotic zone is less than the depth of the mixed layer, light cannot be fully utilized and may prevent full growth of the phytoplankton production from reaching its maximum productivity (Cloern 1987; Brawley et al. 2003; Brush and Brawley 2009). In these shallow areas, the whole water column is usually within the euphotic zone and hence the light availability can often be limited by the water depth. This has been widely observed in different estuaries
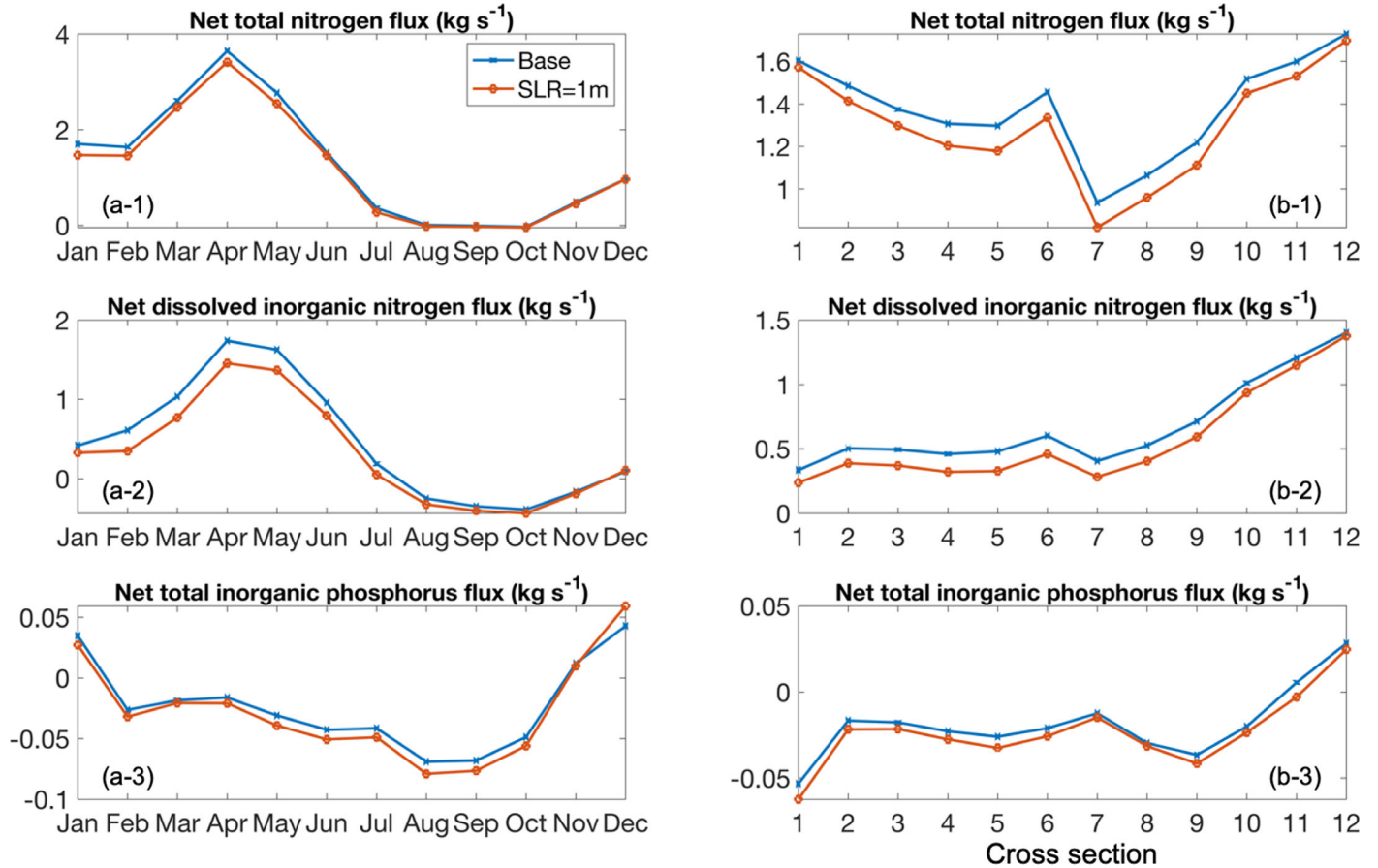
FIGURE 10. (a) Five-year averages of net nutrient flux for each month from 1991 to 1995 at Cross-section 4 near Rappahannock Shoal (Figure 1); (b) Five-year averages of annual net nutrient flux from 1991 to 1995 at the 12 cross-sections Bay mouth to head. Panels (a,b-1) are total nitrogen, panels (a,b-2) are dissolved inorganic nitrogen and panels (a,b-3) are total inorganic phosphorus. Negative values mean flux into the Bay, whereas positive values refer to outflow.

that phytoplankton production is often less than the maximum values in the areas where the water depth is shallower than the euphotic depth (e.g., Cloern 1987; Mallin et al. 1991; Boyer et al. 1993). Thus, in some shallow areas of the tributaries, the increase in water depth and change in hydrodynamics as a result of SLR can have a nontrivial impact on light supply for phytoplankton growth and hence on primary production. This can be examined quantitively using the equation for primary production. The phytoplankton productivity can be expressed as GPP and phytoplankton biomass (Cloern et al. 2014; Qin and Shen 2017), and the depth-integrated phytoplankton GPP is the integral of productivity from the surface to the bottom:

$$\text{GPP} = \int_0^H G_z C_z \, \mathrm{d}z, \qquad (5)$$

where G_z and C_z are the gross growth rate and volumetric biomass at each depth z, respectively. For shallow areas where the water depth is less than the depth of the

mixed layer depth, the phytoplankton can be assumed to be homogeneously distributed at each depth (for the sake of analytical solutions), and the biomass C_z can be assumed to be independent of depth and equal to the depth-averaged biomass. Therefore, depth-integrated phytoplankton production can be expressed as:

$$\text{GPP} = G \cdot C \cdot H, \qquad (6)$$

where G is depth-averaged gross growth rate (day^{-1}), C is depth-averaged phytoplankton biomass (g C/m^3), and H is water depth (m). Under light limitation, gross growth rate $G = G_m \cdot f(I)$, where G_m is the temperature-dependent maximum growth rate (day^{-1}) and $f(I)$ is the daily averaged growth-limitation function for light (Chapra 1997):

$$f(I) = \frac{e}{K_d \cdot H} \cdot \left(e^{-\frac{I_0}{I_{opt}} e^{-K_d \cdot H}} - e^{-\frac{I_0}{I_{opt}}} \right), \qquad (7)$$

K_d is light attenuation coefficient (m^{-1}), I_0 is incident light irradiance at the surface and I_{opt} is
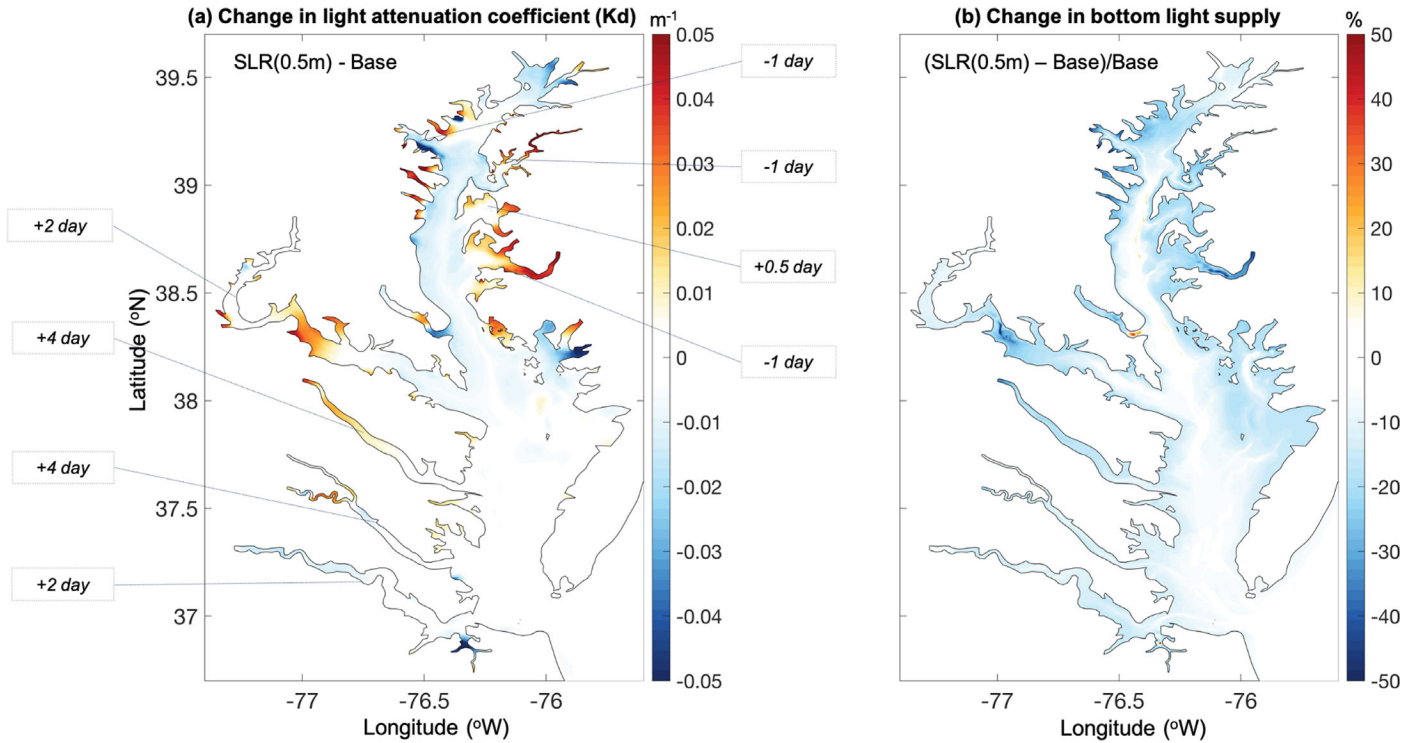
FIGURE 11. (a) Difference of depth-averaged light attenuation coefficient (K_d) caused by SLR of 0.5 m from April to June. Side labels in days indicate the estimated change of flushing time caused by an SLR of 0.5 m for each major tributary. (b) The relative difference of bottom light supply from April to June caused by SLR = 0.5 m on Base Scenario.

optimal light intensity (langleys day^{-1}). Equations (6 and 7) suggest that under SLR, a possible change in GPP can result from changes in water depth, H, light attenuation, K_d, or phytoplankton biomass, C. Substituting Equation (7) into Equation (6) reads:

$$\text{GPP} = G_m \cdot C \cdot \frac{e}{K_d} \cdot \left(e^{-\frac{I_0}{I_{opt}} \cdot e^{-K_d \cdot H}} - e^{-\frac{I_0}{I_{opt}}} \right). \quad (8)$$

The effect of water depth on GPP is through its comparison with the depth of the euphotic zone (denoted by H_u). If water depth $H \geq H_u$, the utilization of the light by phytoplankton in the water column is not limited by the water depth. In this case, light irradiance approaches zero at the bottom. Since light irradiance at each depth z can be described by the Beer–Lambert law, $I(z) = I_0 e^{-k_d \cdot z}$, we have $I(H) = I_0 e^{-k_d \cdot H} \approx 0$. This results that $e^{-k_d \cdot H} \approx 0$ and $e^{-\frac{I_0}{I_{opt}} \cdot e^{-K_d \cdot H}} \approx 1$. Therefore, the daily averaged growth-limiting function for light can be simplified as:

$$f^*(I) = \frac{e}{K_d \cdot H} \left(1 - e^{-\frac{I_0}{I_{opt}}} \right). \quad (9)$$

We used $f^*(I)$ to denote the $f(I)$ when the utilization of the light by phytoplankton in the water column is not limited by the water depth. If the water depth is less than the depth of the euphotic zone, $H < H_u$, i.e., light can penetrate ultimately to the bottom. In this case, the utilization of the light by phytoplankton in the water column is limited by the water depth, $I(H) = I_0 e^{-k_d \cdot H} > 0$ and $e^{-\frac{I_0}{I_{opt}} \cdot e^{-K_d \cdot H}}$ is <1. Obviously, $f(I) < f^*(I)$.

To describe $f(I)$ in the two cases $H \geq H_u$ and $H < H_u$, the daily averaged growth-limiting function for light may be expressed as:

$$f(I) = r \cdot f^*(I), \quad (10)$$

where r is a factor ranging from 0 to 1, and it has the expression:

$$r = \frac{e^{-\frac{I_0}{I_{opt}} \cdot e^{-K_d \cdot H}} - e^{-\frac{I_0}{I_{opt}}}}{1 - e^{-\frac{I_0}{I_{opt}}}}. \quad (11)$$

For the case $H \geq H_u$, $r = 1$ and $f(I) = f^*(I)$. For the case $H < H_u$, $r < 1$, and Equation (11) suggests a positive correlation between r and $K_d \cdot H$. Over shallow areas where the whole water column is within the euphotic zone when the water becomes deeper, more light energy can be utilized in the water column until the local depth exceeds the 1% light level.

Correspondingly, Equation (6) can be expressed explicitly as:

$$\text{GPP} = G_{\text{m}} \cdot r \cdot \frac{e}{K_{\text{d}}} \left(1 - e^{-\frac{I_0}{I_{\text{opt}}}} \right) \cdot C. \qquad (12)$$

Equation (12) suggests that the change of GPP under light limitation due to SLR can be explained quantitatively by the changes in r, C, and K_{d}.

Among the three factors r, C, and K_{d}, the increase in GPP is mainly driven by the increase in r under SLR in the Bay. The model results show that K_{d} is not a major factor in changing GPP. Except in certain areas with an extreme high phytoplankton biomass and particulate organic matter, the main stem and the channel areas of most tributaries exhibit a decrease in light attenuation ($\Delta K_{\text{d}} < 0$) under SLR, but the magnitude of ΔK_{d} is small (<1%; Figure 11a) and its impact on phytoplankton is minor. Changes in phytoplankton biomass C are also not likely a determining factor leading to an increase in GPP in the scenarios. Model results show that the percentage increase in C after SLR is not as high as that in GPP in tributaries, and C even decreases in some locations. The change of biomass C is determined by local and transport processes (Cloern 1996; Qin and Shen 2017; Qin 2019):

$$\frac{dC}{dt} = GC - R_{\text{r}}C - R_{\text{m}}C - \frac{\omega_{\text{c}}}{H}C - FC, \qquad (13)$$

where R_{r} and R_{m} are respiration rate (day^{-1}) and mortality rate (day^{-1}), respectively, ω_{c} is the settling velocity of phytoplankton (m/day), and F is the flushing rate due to transport processes (day^{-1}). In the tributaries, the overall changes in flushing in tributaries are not large compared with their values in Base Scenario, suggesting the increase in C is mainly due to changes in local processes. Among the local processes, respiration and grazing rates are kept unchanged in the model, and the increase in C can only be through an increase in production or a decrease in settling due to an increase in water depth. While it is not clear if the increase in C is mainly due to the increase in GPP or the decrease in settling, the model results show that the increase in C is not the major factor in increasing GPP. Take the Choptank River, which has the largest positive ΔMchla, as an example. The mean water depth of the Choptank River is about 3.95 m, so the change of water depth is about 12.7% under the case of a 0.5 m SLR. In this river, ΔK_{d} is <0.005 m^{-1} over the river channel, which is a small value compared to K_{d} of about 0.4 m^{-1}, and K_{d} decreases <1%. Hence, the combined change in $K_{\text{d}} \cdot H$ increases about 11.6%, which corresponds to an increase in r. Calculations of

model results show that GPP increases about 25% and C increases about 10% after a 0.5 m SLR (Figures 4 and 5), so Equation (12) suggests that the increase in r is about 13.6% under SLR, which is more than that in C or K_{d}. Thus, in those areas where the water depth is less than the depth of the euphotic zone, the increase in GPP is mainly due to the increase in r, and the mechanism that SLR increases GPP is mainly through the increase in the percent of light utilized by phytoplankton in the water column.

The current model does not simulate benthic algae or submerged vegetation. For the areas with abundant benthic producers, the interactions between pelagic and benthic producers can alter the results (Qin and Shen 2019). Under SLR, the elevated depth enhanced GPP in the water column, which could decrease the light supply to the benthic producers. When the SLR is 0.5 m, the overall decrease in light availability at the bottom ranges from 10% to 25% in the shoals where the benthic producers are supported by excess light before SLR (Figure 11b). The bottom light supply experiences little change in deep regions where the benthic producer cannot survive anyway because of the limited light supply. Although the current model does not couple a benthic algal model (e.g., Cerco and Seitzinger 1997) to explicitly estimate the response of the benthic producers to SLR, a reduction of <25% on benthic production is estimated based on the PI curve for benthic algae (Pinckney and Zingmark 1993; Dodds et al. 1999). However, the reduction of benthic production also relies on the nutrient supply and the real irradiance reaching the bottom, so future work is required for this direction.

SUMMARY AND CONCLUSION

We utilized a 3D UG model (SCHISM-ICM) to evaluate the influence of SLR on seasonal hypoxia and phytoplankton production in Chesapeake Bay. Three scenarios (SLR = 0.17 m, SLR = 0.5 m, and SLR = 1.0 m) were assessed based on the calibrated current condition (Base Scenario) (Cai et al. 2020) for the period from 1991 to 1995. Under SLR, the bottom DO was predicted to increase in the deep channel of the mid-lower Bay, but to decrease in other areas. Peak summer HV is estimated to increase by about 2%, 8%, and 16% for these three scenarios, respectively, compared with Base Scenario. SLR drives a total volume change (ΔVol) of 1.96, 5.76, and 11.52 km^3, respectively; and the changes in hypoxia volume (ΔHV) account for about 10%–15% of ΔVol.

Different physical and biological drivers are found to have diverse effects, either positive or negative, on the DO budgets and HV. SLR increases the flux of oxygen-rich water from the ocean into the Bay due to increased gravitation circulation and this tends to improve bottom DO. On the other hand, the enhanced stratification and the enlarged volume below the pycnocline will make it take a longer time for oxygen to be transported from the upper layer to the lower layer of the water column. SLR slightly increases lateral circulation but the minor increase fails to significantly enhance the channel-shoal exchange that refuels oxygen in the channel. In addition to the physical contributions, SLR increases phytoplankton production as a result of longer residence times, stronger stratification, and increased light supply in shallow waters; and the production increases up to 15%, 40%, and 80% for these three SLR scenarios, respectively, which in turn increases the water column DO respiration. The increased phytoplankton production and residence time enhance the settling of organic matter to the lower layer. Consequently, more oxygen is consumed that contributes to the increase in the HV. Overall, this model study suggests that both the altered physical processes and the higher respiration under SLR contribute to the enlarged HV.

Shallow areas in tributaries are highly impacted by SLR since the increased water depths are proportionally large compared with the original depths. The model result shows the largest increase in phytoplankton production occurs in the shallow water regions. The analysis shows that the increase in water depth increases light utilization in shallow areas of many tributaries where the whole water column is within the euphotic zone. This facilitates phytoplankton growth and therefore increases the local production in those areas.

For the sake of simplicity and comparison to other studies, the current study only considered the impact of SLR. For shallow areas and tributaries, other factors can be important as well. Four such factors are the land use (that affects nutrient supply), presence of vegetation (either submerged or emergent), presence of benthic algae, and change in temperature. These complications are left to future studies.

AUTHORS' CONTRIBUTIONS

Xun Cai: Conceptualization; data curation; formal analysis; investigation; methodology; validation; visualization; writing-original draft; writing-review & editing. **Jian Shen:** Conceptualization; methodology; supervision; writing-review & editing. **Yinglong J. Zhang:** Conceptualization; funding acquisition; methodology; project administration; resources; software; supervision; writing-review & editing. **Qubin Qin:** Methodology; writing-review & editing. **Zhengui Wang:** Methodology; software. **Harry Wang:** Software.

LITERATURE CITED

Bever, A.J., M.A. Friedrichs, C.T. Friedrichs, M.E. Scully, and L.W. Lanerolle. 2013. "Combining Observations and Numerical Model Results to Improve Estimates of Hypoxic Volume Within the Chesapeake Bay, USA." *Journal of Geophysical Research: Oceans* 118 (10): 4924–44. https://doi.org/10.1002/jgrc.20331.

Boesch, D.F., L.P. Atkinson, W.C. Boicourt, J.D. Boon, D.R. Cahoon, R.A. Dalrymple, T. Ezer *et al.* 2013. "Updating Maryland's Sea-Level Rise Projections." https://digitalcommons.odu.edu/ccpo_pubs/154/.

Boon, J.D., J.M. Brubaker, and D.R. Forrest. 2010. "Chesapeake Bay Land Subsidence and Sea Level Change: An Evaluation of Past and Present Trends and Future Outlook." https://scholarworks.wm.edu/reports/706/.

Boyer, J.N., R.R. Christian, and D.W. Stanley. 1993. "Patterns of Phytoplankton Primary Productivity in the Neuse River Estuary, North Carolina, USA." *Marine ecology progress series. Oldendorf* 97 (3): 287–97. https://www.int-res.com/articles/meps/97/m097p287.pdf.

Brawley, J.W., M.J. Brush, J.N. Kremer, and S.W. Nixon. 2003. "Potential Applications of an Empirical Phytoplankton Production Model to Shallow Water Ecosystems." *Ecological modelling* 160 (1–2): 55–61. https://doi.org/10.1016/S0304-3800(02)00310-1.

Brush, M.J., and J.W. Brawley. 2009. "Adapting the Light Biomass (BZI) Models of Phytoplankton Primary Production to Shallow Marine Ecosystems." *Journal of Marine Systems* 75(1–2): 227–35. https://doi.org/10.1016/j.jmarsys.2008.10.003.

Cai, X., Y.J. Zhang, J. Shen, H. Wang, Z. Wang, Q. Qin, and F. Ye. 2020. "A Numerical Study of Hypoxia in Chesapeake Bay Using an Unstructured Grid Model: Validation and Sensitivity to Bathymetry Representation." *Journal of the American Water Resources Association* 1–24. https://doi.org/10.1111/1752-1688.12887.

Carton, J.A., and B.S. Giese. 2008. "A Reanalysis of Ocean Climate Using Simple Ocean Data Assimilation (SODA)." *Monthly weather review* 136 (8): 2999–3017. https://doi.org/10.1175/2007MWR1978.1.

Cerco, C.F., and T.M. Cole. 1994. *CE-QUAL-ICM: A Three-Dimensional Eutrophication Model, Version 1.0. User's Guide.* Vicksburgh, MS: US Army Corps of Engineers Waterways Experiments Station.

Cerco, C.F., and S.P. Seitzinger. 1997. "Measured and Modeled Effects of Benthic Algae on Eutrophication in Indian River-Rehoboth Bay, Delaware." *Estuaries* 20 (1): 231–48. https://doi.org/10.2307/1352733.

Chapra, S.C. 1997. *Surface Water-Quality Modeling, McGraw-Hill Series in Water Resources and Environmental Engineering.* New York: McGraw-Hill.

Chassignet, E.P., H.E. Hurlburt, O.M. Smedstad, G.R. Halliwell, P.J. Hogan, A.J. Wallcraft, R. Baraille, and R. Bleck. 2007. "The HYCOM (Hybrid Coordinate Ocean Model) Data Assimilative System." *Journal of Marine Systems* 65 (1–4): 60–83. https://doi.org/10.1016/j.jmarsys.2005.09.016.

Cloern, J.E. 1987. "Turbidity as a Control on Phytoplankton Biomass and Productivity in Estuaries." *Continental Shelf Research* 7 (11–12): 1367–81. https://doi.org/10.1016/0278-4343(87)90042-2.

Cloern, J.E. 1996. "Phytoplankton Bloom Dynamics in Coastal Ecosystems: A Review with Some General Lessons from Sustained Investigation of San Francisco Bay, California." *Reviews of Geophysics* 34(2): 127–68. https://doi.org/10.1029/96RG00986.

Cloern, J.E., S.Q. Foster, and A.E. Kleckner. 2014. "Phytoplankton Primary Production in the World's Estuarine-Coastal Ecosystems." *Biogeosciences* 11 (9): 2477. https://doi.org/10.5194/bg-11-2477-2014.

Dettmann, E.H. 2001. "Effect of Water Residence Time on Annual Export and Denitrification of Nitrogen in Estuaries: A Model Analysis." *Estuaries* 24 (4): 481–90. https://doi.org/10.2307/1353250.

Di Toro, D.M., and J.J. Fitzpatrick. 1993. *Chesapeake Bay Sediment Flux Model. Final Report (No. AD-A-267189/9/XAB).* Mahwah, NJ: Hydroqual Inc.

Diaz, R.J., and R. Rosenberg. 1995. "Marine Benthic Hypoxia: A Review of Its Ecological Effects and the Behavioural Responses of Benthic Macrofauna." *Oceanography and Marine Biology: An Annual Review* 33: 245–303.

Dodds, W.K., B.J. Biggs, and R.L. Lowe. 1999. "Photosynthesis-Irradiance Patterns in Benthic Microalgae: Variations as a Function of Assemblage Thickness and Community Structure." *Journal of phycology* 35 (1): 42–53. https://doi.org/10.1046/j.1529-8817.1999.3510042.x.

Hagy, J.D., W.R. Boynton, C.W. Keefe, and K.V. Wood. 2004. "Hypoxia in Chesapeake Bay, 1950–2001: Long-Term Change in Relation to Nutrient Loading and River Flow." *Estuaries* 27 (4): 634–58. https://doi.org/10.1007/BF02907650.

Hansen, D.V., and M. Rattray, Jr. 1966. "Gravitational Circulation in Straits and Estuaries." https://digital.lib.washington.edu/researchworks/bitstream/handle/1773/16068/M66-76.pdf?sequence=1.

Hilton, T.W., R.G. Najjar, L. Zhong, and M. Li. 2008. "Is There a Signal of Sea-Level Rise in Chesapeake Bay Salinity?" *Journal of Geophysical Research: Oceans* 113 (C9). https://doi.org/10.1029/2007JC004247.

Hong, B., and J. Shen. 2012. "Responses of Estuarine Salinity and Transport Processes to Potential Future Sea-Level Rise in Chesapeake Bay." *Estuarine, Coastal and Shelf Science* 104: 33–45. https://doi.org/10.1016/j.ecss.2012.03.014.

IPCC. 2007. "Summary for Policymakers." In *Climate Change 2007: The Physical Science Basis. Contribution of Working Group I to the Fourth Assessment Report of the Intergovernmental Panel on Climate Change*, edited by S. Solomon, D. Qin, M. Manning, Z. Chen, M. Marquis, K.B. Averyt, M. Tignor and H.L. Miller. Cambridge: Cambridge University Press.

Irby, I.D., M.A. Friedrichs, F. Da, and K.E. Hinson. 2018. "The Competing Impacts of Climate Change and Nutrient Reductions on Dissolved Oxygen in Chesapeake Bay." *Biogeosciences* 15 (9): 2649–68. https://doi.org/10.5194/bg-15-2649-2018.

Kemp, W.M., P. Sampou, J. Caffrey, M. Mayer, K. Henriksen, and W.R. Boynton. 1990. "Ammonium Recycling Versus Denitrification in Chesapeake Bay Sediments." *Limnology and Oceanography* 35 (7): 1545–63. https://doi.org/10.4319/lo.1990.35.7.1545.

Kemp, W.M., P.A. Sampou, J. Garber, J. Tuttle, and W.R. Boynton. 1992. "Seasonal Depletion of Oxygen from Bottom Waters of Chesapeake Bay: Roles of Benthic and Planktonic Respiration and Physical Exchange Processes." *Marine Ecology Progress Series* 85: 137–52. https://doi.org/10.3354/meps085137.

MacCready, P., and W.R. Geyer. 2009. "Advances in Estuarine Physics." *Annual Review of Marine Science* 2: 35–58. https://doi.org/10.1146/annurev-marine-120308-081015.

Mallin, M.A., H.W. Paerl, and J. Rudek. 1991. "Seasonal Phytoplankton Composition, Productivity and Biomass in the Neuse River Estuary, North Carolina." *Estuarine, Coastal and Shelf Science* 32 (6): 609–23. https://doi.org/10.1016/0272-7714(91)90078-P.

Mesinger, F., G. DiMego, E. Kalnay, K. Mitchell, P.C. Shafran, W. Ebisuzaki, D. Jović *et al.* 2006. "North American Regional Reanalysis." *Bulletin of the American Meteorological Society* 87 (3): 343–60. https://doi.org/10.1175/BAMS-87-3-343.

Monsen, N.E., J.E. Cloern, L.V. Lucas, and S.G. Monismith. 2002. "A Comment on the Use of Flushing Time, Residence Time, and Age as Transport Time Scales." *Limnology and Oceanography* 47 (5): 1545–53. https://doi.org/10.4319/lo.2002.47.5.1545.

Murphy, R.R., W.M. Kemp, and W.P. Ball. 2011. "Long-Term Trends in Chesapeake Bay Seasonal Hypoxia, Stratification, and Nutrient Loading." *Estuaries and Coasts* 34 (6): 1293–309. https://doi.org/10.1007/s12237-011-9413-7.

Najjar, R.G., C.R. Pyke, M.B. Adams, D. Breitburg, C. Hershner, M. Kemp, R. Howarth *et al.* 2010. "Potential Climate-Change Impacts on Chesapeake Bay." *Estuarine, Coastal and Shelf Science* 86 (1): 1–20. https://doi.org/10.1016/j.ecss.2009.09.026.

Newcombe, C.L., and W.A. Horne. 1938. "Oxygen-Poor Waters of the Chesapeake Bay." *Science* 88 (2273): 80–81. https://doi.org/10.1126/science.88.2273.80.

Ni, W., M. Li, A. Ross, and R.G. Najjar. 2017. "Downscaling Climate Projections for Chesapeake Bay Hypoxia in the Mid-21st Century." 24th Biennial CERF Conference, CERF.

Nixon, S.w., J.W. Ammerman, L.P. Atkinson, V.M. Berounsky, G. Billen, W.C. Boicourt, W.R. Boynton *et al.* 1996. "The Fate of Nitrogen and Phosphorus at the Land-Sea Margin of the North Atlantic Ocean." *Biogeochemistry* 35 (1): 141–80. https://doi.org/10.1007/BF02179826.

Pinckney, J., and R.G. Zingmark. 1993. "Photophysiological Responses of Intertidal Benthic Microalgal Communities to in Situ Light Environments: Methodological Considerations." *Limnology and Oceanography* 38 (7): 1373–83. https://doi.org/10.4319/lo.1993.38.7.1373.

Qin, Q. 2019. "Impacts of Physical Transport on Estuarine Phytoplankton Dynamics and Harmful Algal Blooms." *Dissertations, Theses, and Masters Projects*. Paper 1550153910. https://doi.org/10.25773/v5-h808-1x32.

Qin, Q., and J. Shen. 2017. "The Contribution of Local and Transport Processes to Phytoplankton Biomass Variability over

Different Timescales in the Upper James River, Virginia." *Estuarine, Coastal and Shelf Science* 196: 123–33. https://doi.org/10.1016/j.ecss.2017.06.037.

Qin, Q., and J. Shen. 2019. "Pelagic Contribution to Gross Primary Production Dynamics in Shallow Areas of York River, VA, USA." *Limnology and Oceanography* 64(4): 1484–99. https://doi.org/10.1002/lno.11129.

Rahmstorf, S. 2007. "A Semi-Empirical Approach to Projecting Future Sea-Level Rise." *Science* 315(5810): 368–70. https://doi.org/10.1126/science.1135456.

Seliger, H.H., J.A. Boggs, and W.H. Biggley. 1985. "Catastrophic Anoxia in the Chesapeake Bay in 1984." *Science* 228 (4695): 70–73. https://doi.org/10.1126/science.228.4695.70.

Shen, J., and L. Haas. 2004. "Calculating Age and Residence Time in the Tidal York River Using Three-Dimensional Model Experiments." *Estuarine, Coastal and Shelf Science* 61 (3): 449–61. https://doi.org/10.1016/j.ecss.2004.06.010.

Shen, J., and J. Lin. 2006. "Modeling Study of the Influences of Tide And Stratification on Age of Water in the Tidal James River." *Estuarine, Coastal and Shelf Science* 68(1–2): 101–12. https://doi.org/10.1016/j.ecss.2006.01.014.

Shenk, G.W., and L.C. Linker. 2013. "Development and Application of the 2010 Chesapeake Bay Watershed Total Maximum Daily Load Model." *Journal of the American Water Resources Association* 49 (5): 1042–56. https://doi.org/10.1111/jawr.12109.

Smith, E.M., and W.M. Kemp. 1995. "Seasonal and Regional Variations in Plankton Community Production and Respiration for Chesapeake Bay." *Marine Ecology Progress Series. Oldendorf* 116 (1): 217–31. https://doi.org/10.3354/meps116217.

St-Laurent, P., M.A.M. Friedrichs, M. Li, and W. Ni. 2019. "Impacts of Sea Level Rise on Hypoxia in Chesapeake Bay: A Model Intercomparison." Report to Virginia Tech and Chesapeake Bay Program, October 2019, 34 pp. https://scholarworks.wm.edu/reports/2310/.

Taft, J.L., W.R. Taylor, E.O. Hartwig, and R. Loftus. 1980. "Seasonal Oxygen Depletion in Chesapeake Bay." *Estuaries* 3 (4): 242–47. https://doi.org/10.2307/1352079.

Vaquer-Sunyer, R., and C.M. Duarte. 2008. "Thresholds of Hypoxia for Marine Biodiversity." *Proceedings of the National Academy of Sciences of the United States of America* 105 (40): 15452–57. https://doi.org/10.1073/pnas.0803833105.

Wang, P., L. Linker, H. Wang, G. Bhatt, G. Yactayo, K. Hinson, and R. Tian. 2017. "Assessing Water Quality of Chesapeake Bay by the Impact of Sea Level Rise and Warming." In IOP Conference Series: Earth and Environmental Science (Volme 82, No. 1, p. 012001). https://iopscience.iop.org/article/ https://doi.org/10.1088/1755-1315/82/1/012001/meta.

Xiong, J., J. Shen, Q. Qin, and J. Du. 2021. "Water Exchange and Its Relationships with External Forcings and Residence Time in Chesapeake Bay." *Journal of Marine Systems* 215: 103497. https://doi.org/10.1016/j.jmarsys.2020.103497.

Zervas, C. 2001. *Sea Level Variations of the United States, 1854–1999* (Volume 36). Silver Spring, MD: US Department of Commerce, National Oceanic and Atmospheric Administration, National Ocean Service.

Zhang, Y.J., E. Ateljevich, H.C. Yu, C.H. Wu, and C.S. Jason. 2015. "A New Vertical Coordinate System for a 3D Unstructured-Grid Model." *Ocean Modelling* 85: 16–31. https://doi.org/10.1016/j.ocemod.2014.10.003.

Zhang, Y.J., F. Ye, E.V. Stanev, and S. Grashorn. 2016. "Seamless Cross-Scale Modeling with SCHISM." *Ocean Modelling* 102: 64–81. https://doi.org/10.1016/j.ocemod.2016.05.002.